

1 **Measurement of light absorbing particles in surface snow of**
2 **central and western Himalayan glaciers: spatial variability,**
3 **radiative impacts, and potential source regions**

4
5 Chaman Gul^{1,2,3,4}, Shichang Kang^{1,4}, Siva Praveen Puppala², Xiaokang Wu⁵, Cenlin He⁶,
6 Yangyang Xu⁵, Inka Koch¹, Sher Muhammad¹, Rajesh Kumar⁶, Getachew Dubache³
7

8 ¹State Key Laboratory of Cryosphere Science, Northwest Institute of Eco-Environment and Resources, Chinese
9 Academy of Sciences, Lanzhou 73000, China

10 ²International Centre for Integrated Mountain Development (ICIMOD), G.P.O. Box 3226, Kathmandu, Nepal

11 ³Reading Academy, Nanjing University of Information Sciences and Technology 219 Ningliu Road, Nanjing,
12 Jiangsu, 210044 China.

13 ⁴University of Chinese Academy of Sciences, Beijing, China

14 ⁵Department of Atmospheric Sciences, Texas A&M University, College Station, TX 77843, USA

15 ⁶Research Applications Laboratory, National Center for Atmospheric Research, Boulder, CO 80301, USA
16
17
18
19

20 Correspondence: Siva Praveen Puppala (sivapraveen.puppala@icimod.org);
21
22

23 **Abstract.** We collected surface snow samples from three different glaciers: Yala, Thana, and Sachin in the central
24 and western Himalayas to understand the spatial variability and radiative impacts of light-absorbing particles. The
25 Yala and Thana glaciers in Nepal and Bhutan, respectively, were selected to represent the central Himalayas. The
26 Sachin glacier in Pakistan was selected to represent the western Himalayas. The samples were collected during the
27 pre-and post-monsoon seasons of the year 2016. The samples were analysed for black carbon (BC) and water-
28 insoluble organic carbon (OC) through the thermal optical method. The average mass concentrations (BC 2381 ng g⁻¹;
29 OC 3896 ng g⁻¹; dust 101 µg g⁻¹) in the western Himalaya (Sachin glacier) were quite high compared to the mass
30 concentrations (BC 358 ng g⁻¹, OC 904 ng g⁻¹, dust 22 µg g⁻¹) at the central Himalaya (Yala glacier). The difference
31 in mass concentration may be due to the difference in elevation, snow age, local pollution sources, and difference in
32 meteorological conditions. BC in surface snow was also estimated through WRF-Chem simulations at the three
33 glacier sites during the sampling periods. Simulations reasonably capture the spatial and seasonal patterns of the
34 observed BC in snow but with a relatively smaller magnitude. Absolute snow albedo was estimated through the
35 Snow, Ice, and Aerosol Radiation (SNICAR) model. The absolute snow albedo reduction was ranging from 0.48 %
36 (Thana glacier during September) to 24 % (Sachin glacier during May) due to BC and 0.13 % (Yala glacier during
37 September) to 5% (Sachin glacier during May) due to dust. The instantaneous radiative forcing due to BC and dust
38 was estimated in the range of 0 to 96.48 W m⁻² and 0 to 25 W m⁻² respectively. The lowest and highest albedo
39 reduction and radiative forcing were observed in central and western Himalayan glaciers, respectively. The potential
40 source regions of the deposited pollutants were inferred using WRF-Chem tagged-tracer simulations. Selected
41 glaciers in the western Himalayas were mostly affected by long-range transport from the Middle East and Central
42 Asia; however, the central Himalayan glaciers were mainly affected by local and South Asia emissions (from Nepal,
43 India, and China) especially during the pre-monsoon season. Overall, South Asia and West Asia were the main
44 contributing source regions of pollutants.

45

46 **Keywords:** black carbon; organic carbon; Yala glacier; Thana glacier; Sachin glacier; snow albedo

47

48

49 **1 Introduction**

50 Black carbon (BC) is a distinct type of carbonaceous material that is formed primarily in flames. BC particles in the
51 atmosphere are generally produced by the incomplete combustion of fossil fuel, biofuel, and biomass. BC is only a
52 minor contributor to aerosol mass but has a great climatic interest as a strong absorber of solar radiation (Quinn et
53 al., 2008; Ramanathan and Carmichael, 2008). In addition to warming, BC particles can interact with clouds,
54 changing their microphysical properties, and thus impacting the climate (Wang et al., 2018; Bond et al., 2013; Dong
55 et al., 2021). Besides this, several studies in the past highlighted the role of BC on the cryosphere (Kang et al., 2019,
56 2020).

57
58 The cryosphere is one of the most sensitive indicators of climate change. The temperature rise in cryospheric regions
59 is generally larger than that in other regions on the global scale (Pepin and Lundquist 2008; Kang et al., 2010; You
60 et al., 2021; Huang et al., 2019). BC particles deposit on the glaciers or snow cover surface, decreasing the surface
61 albedo and absorbing more solar radiation (Warren and Brandt, 2008; He et al., 2017) which accelerates snow and
62 ice melt and triggers albedo feedback (Flanner et al., 2009; Hansen and Nazarenko, 2004; Kang et al., 2020). The
63 forcing produced by BC and other light-absorbing particles (LAPs) further affects the regional climate (Flanner et
64 al., 2009; Xu et al., 2016; Ji et al., 2015) leads to complex responses of the Earth's climate system (Hansen et al.,
65 1997). The largest climate forcing from BC in the snow is estimated to occur over the Tibetan Plateau (TP) and
66 Himalayas (Flanner et al., 2009; Ji et al., 2015).

67
68 Mountain glaciers are the most important freshwater resources to the inhabitants of arid and semi-arid regions
69 (Hock, 2005, 19; Mayer et al., 2006). The Himalayas is considered as world's largest freshwater reservoir outside
70 the Polar Regions (Immerzeel et al., 2010; Marcovecchio et al., 2021). The economy and lives of millions of people
71 in the region are influenced by the changes in mountain river discharge downstream of the Himalayas (Vaux et al.,
72 2012). Lack of in-situ data, the low resolution of emission inventory, and coarse model resolutions prevent an
73 accurate evaluation of LAPs impacts on snow albedo and radiative forcing. Many glaciers have retreated in the
74 region due to climate warming (Zhang et al., 2009; Kang et al., 2010; Yao et al., 2019), and possibly due to LAP-
75 induced surface darkening (Flanner et al., 2009; Qian et al., 2011; Kang et al., 2019). Glacier retreat in the TP and
76 the Himalayan region has serious consequences because snow and runoff from this region are sources of major
77 rivers in Asia, and the availability of freshwater resources has profound effects on human health and agriculture
78 (Immerzeel et al., 2010). However, large uncertainties remain regarding glacier retreat driven predominately by the
79 deposition of BC and other LAPs (Bolch et al., 2012; Kang et al., 2020).

80
81 Snow albedo is an important indicator of surface energy budget over the snow-covered area. Small changes in
82 surface snow albedo can have large impacts on surface warming due to the rapid feedback involving changes to
83 sublimation, snow morphology, and melt rates (Bond et al., 2013). The concentration of LAPs in surface snow is a
84 major factor that affects snow albedo. BC and other LAPs present in the snow reduce the albedo in the visible
85 portion of the electromagnetic spectrum (e.g., Warren and Wiscombe, 1980, Flanner et al., 2007). Besides the

86 concentration of pollutants deposited on the surface of the snow, multiple other factors, such as solar zenith angle
87 (SZA), snow grain size, snow grain shape, snow surface texture, snow density, and snowpack thickness, can also
88 affect snow albedo (He and Flanner, 2020). The radiative transfer model used for the albedo has brought a better
89 understanding of snow optical properties in the shortwave spectrum (He and Flanner, 2020). We estimated the
90 spectral snow albedo using the online Snow, Ice, and Aerosol Radiative (SNICAR) model (Flanner and Zender,
91 2006). The model was originally developed by Flanner et al., 2007, further updated by He et al. (2018) and Dang et
92 al., (2019), and has been widely used in simulating the impacts of LAPs on snow albedos (Qu et al., 2014).

93
94 Here we present the mass concentration of BC, water-insoluble organic carbon (OC), and mineral dust in surface
95 snow from the ablation and accumulation zones of selected glaciers, located in three different countries (Nepal,
96 Bhutan, and Pakistan) on the southern slope of the Himalaya. The Yala and Thana glaciers were selected from the
97 central Himalayas, while the Sachin glacier was selected from the western Himalayas. To reasonably compare the
98 results (mass concentrations, and optical and radiative properties) across the central and western Himalayas, samples
99 were collected on similar dates of the same seasons (pre-monsoon and post-monsoon). We investigate the spatial
100 variability of BC, OC, and mineral dust concentrations due to differences in the source region, meteorology,
101 deposition, and post-deposition processes. The measured mass concentrations were compared to regional model
102 simulations. The associated changes in surface snow albedo and radiative forcing (RF) by mineral dust and BC in
103 surface snow were estimated using the SNICAR model. We also aim to identify the potential source regions of
104 pollution reaching sampling sites using tracer-tagged model simulations.

105 106 **2 Study area and meteorology**

107 Samples were collected from the Yala glacier (28°14' N, 85°37' E) in the Langtang valley of Nepal, the Thana
108 glacier (28°01' N, 90°36' E) in the Chamkhar valley of Bhutan, and the Sachin glacier (35°19' N, 74°45' E) in
109 northern Pakistan (Table 1). Monthly mean surface air temperature and precipitation (MERRA-2 reanalysis data)
110 over the selected glaciers were analyzed and compared for the western and central Himalayan glaciers from April
111 2015 to October 2017 (Table 2). Yala Glacier is a plateau-shaped glacier that has an elevation range between 5160
112 and 5750 m a.s.l. The length of the Yala glacier is 1.5 km facing the northwest. The glacier is located away from the
113 residential area and is mostly covered by firn/snow, especially during the winter season. Details about the
114 metrological condition at the Yala glacier are available in Mukesh et al., (2019) and Gul et al., (2021). Thana glacier
115 is a gentle slope glacier with slight debris cover and an elevation range between 5250 and 5700 m a.s.l. The length
116 of the glacier is about 5 km, facing the southwest. The Thana glacier is mostly covered by fresh snow especially
117 during the winter season. The Sachin glacier has a gentle slope with dense debris cover in its ablation area with an
118 altitude range from 3105 to 4976 m a.s.l. The length of the Sachin glacier is around 8 km facing northeast. In
119 general, the Sachin is a low elevation and relatively debris-covered glacier compared to the central Himalayan
120 glaciers (Yala and Thana). Precipitation in central Himalayan glaciers (Yala and Thana) was higher than that of the
121 western Himalayan glacier (Sachin) especially from April to October each year (Table 2). Surface air temperature
122 over the Yala and Sachin glacier was higher than that of the Thana glacier. The geographical location of the selected

123 glaciers and snow sampling locations are shown in Fig. 1. Besides the difference in altitude, latitude, and
124 meteorology of the selected glaciers in the central and western Himalayas, there is also a difference in the surface
125 condition shown in supplementary Fig. S1.

126

127 **3 Methodologies**

128

129 **3.1 Snow sampling and analysis**

130 Surface snow samples were collected from the central and western Himalayan glaciers during May, and September
131 2016. Samples were taken from the ablation and accumulation zones of the selected glaciers; however, a few snow
132 samples were also collected from the surrounding nearby areas of the Yala and Sachin glaciers. Sachin glacier's
133 samples were relatively aged snow and had less snow thickness as compared to the samples collected from Thana
134 and Yala glaciers (supplementary Fig. S1). At each sampling location, Whirl-Pak bags were used to collect samples
135 from the upper 0-10 cm of depth (approximately 2 L, unmelted). The samples were kept frozen until they were
136 melted and filtered in through the quartz filters near the sampling site. The snow density was measured with a small
137 density kit. The snow grain size was measured through a hand lens (25×) with an accuracy of 0.02mm. The same
138 sampling protocol was used for all the three selected glaciers. A detailed description of the sampling procedure is
139 described in Li et al.,2016a. Quartz filters were used to measure the mass concentration of BC, OC, and dust in the
140 collected samples. BC and OC present in snow samples were analyzed by a filter-based thermal-optical analysis
141 method using DRI® Model 2005 (Chow et al., 1993). Filters were analyzed at the State Key Laboratory of
142 Cryosphere Science, Northwest Institute of Eco-Environment and Resources, Chinese Academy of Sciences. Before
143 starting the analysis, a piece of the sampled filters was put in an oven for a few minutes to eliminate the water vapor
144 content and volatile organic compounds. Further detailed information on the instrument and analysis method can be
145 referred to in earlier studies (Gul et al., 2018).

146

147 **3.2 Estimation of snow albedo reduction and radiative forcing**

148 The online snow simulation model SNICAR (Flanner et al., 2007, <http://snow.engin.umich.edu/>) was used to
149 estimate snow albedo calculation for the collected samples. The model has been used by multiple studies in the past
150 (e.g., Li et al., 2017; Gul et al., 2018; Zhang et al., 2018). Albedo was simulated based on an hourly SZA at the
151 sampling site with an averaged mass concentration of BC, dust, and other input parameters such as snow grain size,
152 snow density, and snow depth from measurements. We computed broadband snow albedo for direct solar incident
153 radiation under the mid-latitude winter clear sky condition, (Supplementary Table S1). Depending on geographical
154 location, 10 to 15 SZAs were used (between 0° and 90°) during instantaneous daytime albedo simulation. Albedo
155 was simulated in four categories: 1- broadband albedo with BC and dust in snow, 2- broadband albedo with BC in
156 snow only, 3- broadband albedo with dust in snow only, and 4- broadband albedo with the absence of BC and dust
157 which was considered as a reference albedo. Radiative implications caused by snow darkening due to BC and dust
158 deposition were investigated using the albedo reduction and the radiative transfer model Santa Barbara DISORT
159 Atmospheric Radiative Transfer (SBDART) (Ricchiazzi et al., 1998). To evaluate the amount of additional solar

160 radiations absorbed by the snow in the presence of BC and dust, we estimated the mean solar irradiance and its
161 characteristics via SBDART, which has been used in the past (Yang et al., 2015). According to the location of the
162 sampling site, the characteristics of the atmospheric profiles such as water vapor, aerosols, ozone, etc. were set in the
163 model. RF for the snow samples was estimated by following Eq. (1):

$$164 \quad RF_x = R_{in-short} * \Delta \alpha_x \quad (1)$$

165 where, $R_{in-short}$ denotes incident short-wave solar radiation for selected SZA and $\Delta \alpha_x$ denotes the reduction in albedo
166 due to BC, dust, or both, as simulated by the SNICAR model.

167

168 **3.3 Potential source region of pollutants**

169 Glaciers of the Himalaya Karakoram and Hindukush (HKH) region are located at high altitudes as compared to the
170 sources of the major pollutants. LAPs including BC and dust can transport from urban areas toward glaciated areas
171 (e.g., Yasunari et al., 2009; Kang et al., 2019). Multiple approaches, including climate circulation modeling,
172 combinations of bottom-up inventories, and back air trajectories have been used in the past to determine the possible
173 source regions of pollution in the HKH region. To identify the potential source region of pollution arriving at the
174 observation sites, we used the weather research and forecasting (WRF) model coupled with chemistry (WRF-Chem
175 version 3.9.1.1) simulations (Grell et al., 2005). The model uses region-tagged tracers for different regions across the
176 world.

177

178 WRF-Chem simulations were used to estimate BC mass concentration in surface snow and deposition of BC
179 particles on three selected glaciers (Yala, Thana, and Sachin). We archived the hourly model results for
180 instantaneous BC deposition and concentration in snow. The horizontal grid spacing of the model was 20 km x 20
181 km with 35 vertical levels stretching from the surface up to 50 hPa (~20 km). The updated Model for Ozone And
182 Related chemical Tracers (MOZART) was applied for the gas phase chemistry (Knote et al., 2014) while aerosols in
183 the WRF-Chem were simulated via the Model for Simulating Aerosol Interactions and Chemistry (MOSAIC)
184 (Zaveri et al., 2008). We use the Global Data Assimilation System (GDAS) from the National Center for
185 Environmental Prediction (NCEP) for the meteorological initial and boundary conditions. We used the Fire
186 Inventory from NCAR (FINN), the EDGAR-HTAP, and MEGAN (Model of Emissions of Gases and Aerosols from
187 Nature) for biomass burning emissions, anthropogenic emissions, and online biogenic emissions, respectively. For
188 chemical boundary conditions, we used the NCAR global CAM-Chem simulation dataset
189 (<https://rda.ucar.edu/datasets/ds313.7/>). Key meteorological variables such as winds, temperature, and water vapor
190 above the planetary boundary layer (PBL) were nudged every 6 hours towards the NCEP GDAS reanalysis fields to
191 reduce temporal error growth in meteorological variables. We used the Community Land Model (CLM) scheme for
192 the land component in WRF-Chem. The CLM model can simulate BC concentration in snowpack and its effects on
193 snow albedo (Flanner et al., 2007). We used online coupled BC deposition fluxes from the atmosphere component
194 of WRF-Chem with the CLM model following Zhao et al. (2014). We also implemented a tagged-tracer method
195 (Kumar et al., 2015) to track anthropogenic BC emissions from 10 different Asian countries surrounding the TP
196 areas, as well as BC emissions from Asian biomass burning and the domain boundary (i.e., areas outside Asia). The

197 tracked 10 anthropogenic emission source regions include China, India, Nepal, Pakistan, Afghanistan, Bhutan,
198 Bangladesh, Myanmar, Southeast Asia, and the rest of Asia. The aim of the model simulation was to estimate the
199 BC mass concentration in surface snow, deposition of BC particles, and the source contribution to BC deposition on
200 snow.

201

202 **4. Results and discussions**

203 **4.1 Concentrations of light-absorbing particles in surface snow**

204 The average mass concentration of LAPs in surface snow of the Yala glacier was 358 ng g⁻¹ for BC, 904 ng g⁻¹ for
205 OC, and 22 µg g⁻¹ for dust in spring (May) and was relatively lower concentrations of 69 ng g⁻¹ for BC, 177 ng g⁻¹
206 for OC and 4 ng g⁻¹ for dust during autumn (September). These mass concentrations of BC and OC in surface snow
207 were comparable to the study result conducted on the Yala glacier in May 2017 (Gul et al., 2021).

208 High LAP concentration in the pre-monsoon is due to an effective transport mechanism from the Indian
209 subcontinent and an additional source such as forest fires (Gul et al., 2021). The average surface concentrations of
210 BC, OC, and dust in the Thana glacier samples during the autumn season were 39 ng g⁻¹, 115 ng g⁻¹ and 34 µg g⁻¹,
211 respectively. Possible reasons for the lower concentration at the Thana glacier may be due to the relatively high
212 elevation of the sampling location and relatively fresh snow. A strong effect of LAPs (BC and dust) has been
213 observed at lower elevations in comparison to higher elevations (Li et al., 2017). The average concentration of BC,
214 OC, and dust measured in the selected western Himalayan glacier (Sachin) during May were 2381 ng g⁻¹, 3896 ng g⁻¹
215 and 101 µg g⁻¹, respectively, and were relatively higher during October with values of 5314 ng g⁻¹ for BC, and 546
216 µg g⁻¹ for dust (Gul et al., 2018). The observed average mass concentrations in the western Himalayas were higher
217 than those in the central Himalayas. The BC mass concentration difference might be due to the difference in snow
218 type, precipitation rate, local emission, the elevation of sampling sites, meteorology, and BC deposition over the
219 glacier surfaces. Post dry deposition of LAPs over the surface of the snow was an important factor. The pollutants
220 source regions for the central and western Himalayas are different. In the case of central Himalayas, pollutants
221 emitted during pre-monsoon convection and multiple forest fires events are effectively lifting and transported
222 towards central Himalayan glaciers. Due to strong inversion in winter, most of the pollutants get stuck near-surface
223 whereas in monsoon pollutants get scavenged by rain. Thus pre-monsoon is a very significant period in the transport
224 process in the central Himalayas. Snow samples collected from the western side of the Himalayas were aged as
225 compared to the central side; post-deposition ion (or enrichment) of LAPs over the snow surface increased the
226 concentration in the snow (Kang et al., 2019). The majority of the samples from the western Himalayan side were
227 from ablation zones of the glacier, where concentrations of LAPs are higher as compared to the accumulation zone
228 of the glacier. Li et al., (2017) showed a strong negative relationship between the elevation of glacier sampling
229 locations and the concentration of LAPs. Therefore strong melting of surface snow and ice in the glacier ablation
230 zone could lead to BC enrichment which causes high BC concentrations (Li et al., 2017). In the case of western
231 Himalayan glaciers sites, snow samples were collected long after the snowfall and the concentration of pollutants
232 would also have increased in the surface snow due to dry deposition. The surface concentrations of the individual
233 samples collected from the Yala, Thana, and Sachin glaciers during May and September 2016 are shown in Fig. 2,

234 and Table S2. BC and OC concentration on our selected glaciers with a comparison to other glaciers of TP and the
235 surrounding region are shown in Fig. 3 and Table S3. It was observed that the concentration of BC, OC, and dust in
236 the central Himalayan glaciers (Yala and Thana) were comparable to other reported results. In the past, similarly
237 high concentrations were reported in the region (Xu et al., 2012) such as Tien Shan Mountains (Li et al., 2016),
238 Northeast of the TP (Wang et al., 2016), Northern China (Zhang et al., 2016) Southeastern TP, western Tien Shan
239 and Central Asia (Zhang et al., 2017).

240
241 The yellow boxes of Fig. 2 show the WRF-Chem modeled BC concentrations in surface snow at the three
242 measurement glacier sites during the measurement periods. Compared to the observations red boxes in Fig. 2, model
243 results reasonably capture the spatial and seasonal patterns and variables of the observed BC in the snow with a
244 relatively smaller magnitude. The modeled variation at the Sachin site during the October sampling periods is much
245 larger than the observations (Gul et al., 2018). The discrepancies between model results and observations are due to
246 model uncertainties from (1) the relatively coarse grid spacing that may not capture the transport over the complex
247 TP terrain, (2) the underestimated anthropogenic emissions that are not representative of the measurement periods,
248 and (3) deficiencies in model physical parameterizations that affects BC transport and deposition. The WRF-Chem
249 model implicitly accounts for the surface impurity enrichment during snow ablation by using a low meltwater
250 scavenging efficiency for BC. However, we notice that this meltwater scavenging efficiency parameter could be
251 associated with large uncertainties (Qian et al., 2014) due to the lack of direct observational constraints. We also
252 note that the observed variation at each site shown in Fig. 2 includes both the temporal and subgrid variabilities
253 derived from multiple sampling locations surrounding each site (Fig. 1). In contrast, all the measurement locations at
254 each particular glacier site are located within a single model grid. As a result, the model is unable to resolve this
255 subgrid information and hence only includes the temporal variability for each selected site.

256

257 **4.2 Surface snow albedo and radiative forcing**

258 The minimum daytimes absolute albedo reduction due to combined BC and dust, BC only and dust only were in the
259 range (1.03-13.44%), (0.48-12.42%) and (0.12-2.12%), respectively. The maximum daytime albedo reduction due to
260 combined BC and dust, BC only and dust only was in the range (1.98-24.97%), (1.05-24%), and (0.25-4.8%)
261 respectively. The lowest and highest contributions in albedo reduction were observed in the central Himalayas
262 (September) and the western Himalayas (May) respectively. Snow albedo reduction (%) derived from samples
263 collected from the Yala glacier (during May 2016) and the Thana glacier (during September 2016) were in the range
264 of (0.13-3.82%) and (0.90-1.99%), respectively. A significant difference in daytime albedo reduction between the
265 western and central Himalayas was mainly due to the difference in mass concentrations of pollutants and snow age.
266 The pollutant concentrations in the western Himalayan samples (Sachin glacier) were higher, resulting in higher
267 albedo reduction as compared to the central Himalayan (Yala and Thana glaciers) samples. The average elevation
268 difference between central and western sampling sites was greater than 1000 meters, where a high concentration of
269 pollution is expected at the low elevated glacier of the western side as compared to the central side of the Himalaya.
270 Snow samples collected on the central side of the Himalayas (Yala glacier) were much fresher as compared to the

271 samples collected from the western side (Sachin glacier). Dust and other pollutants were visible over the surface of
272 the Sachin glacier (Fig. S1). Aged snow had increased density, enlarged grain size, and increased concentration of
273 BC and dust particles due to dry deposition on the snow surface. In the case of all sampling sites impact of BC on
274 snow albedo reduction was greater than the impact of dust except the Thana glacier where the impact of dust was
275 higher than that of BC (Fig. 4a). This may be due to a different dust type in Thana samples. Daytime snow albedo
276 reductions (%) due to BC only, dust only, and both BC and dust are given in Fig. 4a.

277
278 The daytime instantaneous RF ($W m^{-2}$) ranged from (0.076 to 39.65) for the Yala glacier in May 2016, 0.006 to
279 18.26 for the Yala glacier in September 2016, 0.0 to 11.48 for the Thana glacier in September 2016, and 0.03 to
280 96.48 for the Sachin glacier during May 2016. RF for the western Himalayas (Sachin glacier) was quite high as
281 compared to the central Himalayan glaciers (Yala and Thana glaciers). The radiative effect on the Sachin glacier
282 was much more than that of other selected glaciers mainly due to low albedo and increased temperature. Zhang et al.
283 (2017) reported that a reduction in albedo by 9 to 64 % can increase the instantaneous RF by as much as 24.05–
284 323.18 $W m^{-2}$. In the case of all sampling sites impact of BC on RF was greater than the impact of dust except the
285 Thana glacier where the impact of dust was higher than that of BC (Fig. 4b). Therefore, BC can be a major
286 responsible pollutant in the snow to reduce albedo and increase warming in the selected glaciers. BC was the
287 dominant factor in snow melting in the Yala and Sachin glaciers; however, dust was the dominant factor in Thana
288 glacier samples. According to (Kaspari et al., 2014), RF caused by mineral dust was greater than that of dust. The
289 BC and dust had low importance for RF in fresh snow (central Himalaya - Thana glacier) as compared to aged snow
290 (western Himalaya - Sachin glacier). In the northern TP, BC played important role in RF (Li et al., 2016a), while in
291 the central TP and Himalayas dust was more important than BC (Kaspari et al., 2014). The average instantaneous
292 RF caused by the combined contribution of BC and dust (BC + dust), only BC, and only dust is shown in Fig. 4b as
293 a function of surface snow types. Variation in the RF and albedo change for a particular pollutant type was due to
294 variation in SZA.

295

296 **5 Potential source regions of pollutants**

297 Figure 5 shows the contributions of different BC emission sources to the BC in snow from WRF-Chem tagged-
298 tracer simulations. For the Yala site, it is dominated (>50%) by anthropogenic emissions from India and Nepal for
299 both May and October, while the biomass burning contribution (>20%) increases largely in May primarily due to the
300 spring burning activities in northern India (Kumar et al., 2011). In September, China's contribution also increases to
301 >20% at Yala. For the Thana site, it is dominated (>60%) by anthropogenic emissions from China and India in
302 September, while anthropogenic emissions from Bhutan and Myanmar also contribute about 10%, respectively. The
303 Sachin site is predominantly affected by anthropogenic emissions from India and Pakistan (total contribution
304 >80%), while the spring biomass burning only contributes to ~10% in May. Overall, the source contributions show
305 large variation depending on the site locations and sampling seasons, but with a consistent India contribution of 20-
306 40% across all the sites and seasons.

307

308 **6 Discussion on uncertainty in measurements, albedo, and potential source identification of pollutants**

309 The possible uncertainties in the present research were related to measurements, sampling, analysis, albedo, and RF
310 estimation. A sampling at remote rural sites, sample preservation, filtration, and transport can modify the results if
311 proper standard protocols were not followed. During laboratory analysis via thermal optical techniques, several
312 uncertainties may be related to separating OC from BC in the sample (Gul et al., 2021). The level of generated
313 uncertainty depended on temperature protocol, sample type (residential cookstoves, diesel exhaust, rural aerosols,
314 and urban aerosols), the amount of dust loading on the filter, and the analysis method. The overall accuracy in the
315 measurement of OC, BC, and total carbon concentrations was estimated considering the mass contributions from
316 field blanks and the analytical accuracy of concentration measurements. The uncertainty of the OC and BC mass
317 concentrations was extracted through the standard deviation of the field blanks (Li et al., 2021). OC in snow can
318 produce minor warming (Yasunari et al., 2015), but in this research albedo reduction from OC was not quantified. In
319 albedo simulation and RF estimations, snow grain size and texture can produce large uncertainty. We
320 measured/considered the physical grain size in this research which is not the same as the effects than optical grain
321 size. Optical grain size defines the amount of solar radiation absorbed/scattered by the snow. We assumed a
322 spherical shape for the snow grains which may affect the results because the albedo of non-spherical grains is higher
323 than the albedo of spherical grains (Dang et al., 2016; He et al., 2018). The contribution of pollutants generated from
324 local sources can be important (e.g., Li et al., 2021), which however was not included in the global emission
325 inventories; we were unable to capture emissions at the local scale. Therefore contributions of local sources may be
326 underestimated by coarse-resolution models. High-resolution models and emission inventories at the local scale are
327 required to capture local emissions.

328

329 **7 Conclusions**

330 The average mass concentration of LAPs in the samples collected from the Sachin, Yala, and Thana glaciers were in
331 the range (835 ng g⁻¹ to 3545 ng g⁻¹ for BC and 35 µg g⁻¹ to 253 µg g⁻¹ for Dust), (23 ng g⁻¹ to 2529 ng g⁻¹ for BC
332 and 1.5 µg g⁻¹ to 196 µg g⁻¹ for Dust), and (21 ng g⁻¹ to 127 ng g⁻¹ for BC and 1.5 µg g⁻¹ to 67 µg g⁻¹ for Dust)
333 respectively. Overall the concentrations of BC and dust varied from 21 ng g⁻¹ and 1.5 µg g⁻¹ in fresh snow to 3545
334 ng g⁻¹ and 253 µg g⁻¹ in the aged snow, respectively. Mass concentrations of BC, OC, and dust in the samples
335 collected from the western Himalayas was much higher than the average concentration in the central Himalayas
336 mainly due to difference in snow age, elevation, and meteorology. The accumulation area of glaciers (e.g. ice cores
337 and snow pits), where enrichment influences are less marked and measured values are likely to be lower, and high
338 elevation areas, where deposition of pollutants is expected to be lower. Pollutant concentrations were likely
339 underestimated in the earlier studies, particularly when there was strong surface melting. Dust and other pollutants
340 were visible on aged snow surfaces in the western Himalayan glacier, indicating considerable enrichment during
341 snow aging. WRF-Chem modeled BC concentrations in surface snow were almost similar to the observed BC in the
342 snow with a relatively smaller magnitude.

343

344 Based on observed pollutants, snow albedo reduction (%) in the central Himalayas was in the range of (0.48-3.6%
345 for BC) and (0.13-1.99% for Dust), much lower than that of the western Himalayas. BC was the major component
346 responsible for the albedo reduction, and the dust had little effect except in the Thana glacier. In case the of the
347 Thana glacier, the impact of dust was higher than that of BC. The daytime instantaneous radiative forcing ($W m^{-2}$)
348 ranged from 0.076 to 39.65 (Yala glacier during May 2016), 0.006 to 18.26 (Yala glacier during September 2016),
349 0.0 to 11.48 (Thana glacier during September 2016), 0.03 to 96.48 (Sachin glacier during May 2016). The average
350 albedo reduction due to the combined effect of dust and BC at the western Himalayan side (Sachin glacier) was
351 0.372 which was ~15 times higher than that of the central Himalayan side (Yala glacier). Similarly, the radiative
352 forcing in the western Himalayas was ~6 times higher than that of the central Himalayan side. Observation showed
353 that the potential source regions of pollutants for the western and central Himalayas were different. Western
354 Himalayan glaciers were mostly affected by long-range transport via the westerlies; however central Himalayan
355 glaciers were affected by relatively local winds from Nepal, Bhutan, India, and China. For the western Himalayan
356 glaciers, the emissions from central Asian and South Asian countries (Particularly Pakistan and India) are more
357 important source regions.

358

359 **Acknowledgment**

360 This study was supported by the National Natural Science Foundation of China (41630754), the Chinese Academy
361 of Sciences (XDA20040501, QYZDJ-SSW-DQC039), and the State Key Laboratory of Cryosphere Science
362 (SKLCS-ZZ-2021). This study was also partially supported by the core funds of ICIMOD contributed by the
363 governments Afghanistan, Australia, Austria, Bangladesh, Bhutan, China, India, Myanmar, Nepal, Norway,
364 Pakistan, Sweden, and Switzerland. We thank Faiza Gul, Aditi Mukherji, and Arnico Panday for their useful
365 comments and guidance. We are also grateful to the staff of the National Centre for Hydrology and Meteorology in
366 Bhutan for organizing the Thana Glacier expedition in 2016. We would like to acknowledge high-performance
367 computing support from Cheyenne provided by NCAR's Computational and Information Systems Laboratory,
368 sponsored by the National Science Foundation. NCAR is operated by the University Corporation for Atmospheric
369 Research under the sponsorship of the National Science Foundation.

370

371 **References**

- 372 Bolch, T., Kulkarni, A., Kääb, A., Huggel, C., Paul, F., Cogley, J. G., Frey, H., Kargel, J. S., Fujita, K., Scheel, M.,
373 Bajracharya, S., and Stoffel, M.: The State and Fate of Himalayan Glaciers, *Science*, 336, 310–314, 2012.
- 374 Bond, T. C., Doherty, S. J., Fahey, D. W., Forster, P. M., Berntsen, T., DeAngelo, B. J., Flanner, M. G., Ghan, S.,
375 Kärcher, B., Koch, D., Kinne, S., Kondo, Y., Quinn, P. K., Sarofim, M. C., Schultz, M. G., Schulz, M.,
376 Venkataraman, C., Zhang, H., Zhang, S., Bellouin, N., Guttikunda, S. K., Hopke, P. K., Jacobson, M. Z., Kaiser,
377 J. W., Klimont, Z., Lohmann, U., Schwarz, J. P., Shindell, D., Storelvmo, T., Warren, S. G., and Zender, C. S.:
378 Bounding the role of black carbon in the climate system: A scientific assessment, *J. Geophys. Res.-Atmos.*, 118,
379 5380–5552, doi:10.1002/jgrd.50171, 2013.

380 Chow, J. C., Watson, J. G., Pritchett, L. C., Pierson, W. R., Frazier, C. A., and Purcell, R. G.: The DRI
381 thermal/optical reflectance carbon analysis system: description, evaluation, and applications in US air quality
382 studies, *Atmos. Environ. A-Gen.*, 27, 1185–1201, 1993.

383 Dang, C., Zender, C. S., and Flanner, M. G. (2019), Intercomparison and improvement of twostream shortwave
384 radiative transfer schemes in Earth system models for a unified treatment of cryospheric surfaces, *The*
385 *Cryosphere*, 13, 2325–2343, doi:10.5194/tc-13-2325-2019, 2019.

386 Dang, C., Fu, Q., and Warren, S. G.: Effect of snow grain shape on snow albedo, *J. Atmos. Sci.*, 73, 3573–
387 3583, <https://doi.org/10.1175/JAS-D-15-0276.1>, 2016.

388 Flanner, M. G. and Zender, C. S.: Linking snowpack microphysics and albedo evolution, *J. Geophys. Res. Atmos.*,
389 111(12), 1–12, doi:10.1029/2005JD006834, 2006.

390 Flanner, M. G., Zender, C. S., Randerson, J. T. and Rasch, P. J.: Present-day climate forcing and response from black
391 carbon in snow, *J. Geophys. Res. Atmos.*, 112(11), 1–17, doi:10.1029/2006JD008003, 2007.

392 Flanner, M. G., Zender, C. S., Hess, P. G., Mahowald, N. M., Painter, T. H., Ramanathan, V. and Rasch, P. J.:
393 Springtime warming and reduced snow cover from carbonaceous particles, *Atmos. Chem. Phys. Discuss.*, 8(6),
394 19819–19859, doi:10.5194/acpd-8-19819-2008, 2009.

395 Grell, G. A., Peckham, S. E., Schmitz, R., McKeen, S. A., Frost, G., Skamarock, W. C., and Eder, B.: Fully coupled
396 “online” chemistry within the WRF model, *Atmos. Environ.*, 39, 6957–6975, 2005.

397 Gul, C., Puppala, S.P., Kang, S., Adhikary, B., Zhang, Y., Ali, S., Li, Y., Li, X., 2018. Concentrations and source
398 regions of light-absorbing particles in snow/ice in northern Pakistan and their impact on snow albedo. *Atmos.*
399 *Chem. Phys.* 18, 4981–5000. <https://doi.org/10.5194/acp-18-4981-2018>

400 Gul, C., Mahapatra, P.S., Kang, S., Singh, P.K., Wu, X., He, C., Kumar, R., Rai, M., Xu, Y., Puppala, S.P., Black
401 carbon concentration in the central Himalayas: impact on glacier melt and potential source contribution,
402 *Environmental Pollution*, <https://doi.org/10.1016/j.envpol.2021.116544>, 2021

403 Hansen, J. and Nazarenko, L.: Soot climate forcing via snow and ice albedos, *Proc. Natl. Acad. Sci. U. S. A.*, 101(2),
404 423–428, doi:10.1073/pnas.2237157100, 2004.

405 Hansen, J., Sato, M. & Ruedy, R.: Radiative forcing and climate response, *J. Geophys. Res.* 102 , 6831–6864 ,
406 doi.org/10.1029/96JD03436 ,1997

407 He, C., Flanner, M. G., Chen, F., Barlage, M., Liou, K.-N., Kang, S., Ming, J., and Qian, Y.: Black carbon-induced
408 snow albedo reduction over the Tibetan Plateau: uncertainties from snow grain shape and aerosol–snow mixing
409 state based on an updated SNICAR model, *Atmos. Chem. Phys.*, 18, 11507–11527, [https://doi.org/10.5194/acp-](https://doi.org/10.5194/acp-18-11507-2018)
410 18-11507-2018, 2018

411 He, C., & Flanner, M. (2020). Snow Albedo and Radiative Transfer: Theory, Modeling, and
412 Parameterization. Kokhanovsky A, editor, 67-133.

413 He, C., Takano, Y., Liou, K. N., Yang, P., Li, Q., & Chen, F. (2017). Impact of snow grain shape and black carbon–
414 snow internal mixing on snow optical properties: Parameterizations for climate models. *Journal of*
415 *Climate*, 30(24), 10019-10036. doi:10.1175/JCLI-D-17-0300.1

416 Hock R.: Glacier melt: a review of processes and their modelling. *Progr. Phys. Geogr.*, 29(3), 362–391, doi:

417 10.1191/0309133305pp453ra, 2005.

418 Hock, R., G. Rasul, C. Adler, B. Cáceres, S. Gruber, Y. Hirabayashi, M. Jackson, A. Käb, S. Kang, S. Kutuzov, Al.
419 Milner, U. Molau, S. Morin, B. Orlove, and H. Steltzer, 2019: High Mountain Areas. In: *IPCC Special Report on*
420 *the Ocean and Cryosphere in a Changing Climate* [H.-O. Pörtner, D.C. Roberts, V. Masson-Delmotte, P. Zhai,
421 M. Tignor, E. Poloczanska, K. Mintenbeck, A. Alegría, M. Nicolai, A. Okem, J. Petzold, B. Rama, N.M. Weyer
422 (eds.)]. In press.

423 Immerzeel, W. W., van Beek, L. P. H. and Bierkens, M. F. P.: Climate change will affect the Asian water towers.,
424 *Science*, 328(5984), 1382–5, doi:10.1126/science.1183188, 2010.

425 Ji Z., S. Kang, Z. Cong, Q. Zhang, T. Yao. 2015. Simulation of carbonaceous aerosols over the Third Pole and
426 adjacent regions: distribution, transportation, deposition, and climatic effects. *Climate Dynamics*, 45(9-10):
427 2831-2846. <https://doi.org/10.1007/s00382-015-2509-1>.

428 Kang S., Y. Zhang, Y. Qian, H. Wang. 2020. A review of black carbon in snow and ice and its impacts on
429 cryospheric change. *Earth-Science Reviews*, 210, 103346. <https://doi.org/10.1016/j.earscirev.2020.103346>.

430 Kang S., Q. Zhang, Y. Qian, Z. Ji, C. Li, Z. Cong, Y. Zhang, J. Guo, W. Du, J. Huang, Q. You, A. K. Panday, M.
431 Rupakheti, D. Chen, Örjan Gustafsson, M. H. Thiemens, D. Qin. 2019. Linking Atmospheric Pollution to
432 Cryospheric Change in the Third Pole Region: Current Progresses and Future Prospects. *National Science*
433 *Review*, 6(4): 796-809. <https://doi.org/10.1093/nsr/nwz031>.

434 Kang S., X. Wei, Q. You, Wolfgang-Albert Flügel, Nick Pepin, T. Yao. 2010. Review of climate and cryospheric
435 change in the Tibetan Plateau. *Environmental Research Letter*, 5(2010) 015101 (8pp).
436 <https://doi.org/10.1088/1748-9326/5/1/015101>.

437 Kaspari, S., Painter, T. H., Gysel, M., Skiles, S. M. and Schwikowski, M.: Seasonal and elevational variations of
438 black carbon and dust in snow and ice in the Solu-Khumbu, Nepal and estimated radiative forcings, *Atmos.*
439 *Chem. Phys.*, 14(15), 8089–8103, doi:10.5194/acp-14-8089-2014, 2014.

440 Knote, C., Hodzic, A., Jimenez, J. L., Volkamer, R., Orlando, J. J., Baidar, S., Brioude, J., Fast, J., Gentner, D. R.,
441 Goldstein, A. H., Hayes, P. L., Knighton, W. B., Oetjen, H., Setyan, A., Stark, H., Thalman, R., Tyndall, G.,
442 Washenfelder, R., Waxman, E., and Zhang, Q.: Simulation of semi-explicit mechanisms of SOA formation from
443 glyoxal in aerosol in a 3-D model, *Atmos. Chem. Phys.*, 14, 6213–6239, doi:10.5194/acp-14-6213-2014, 2014.

444 Kumar, R., Barth, M. C., Nair, V. S., Pfister, G. G., Suresh Babu, S., Satheesh, S. K., Krishna Moorthy, K.,
445 Carmichael, G. R., Lu, Z., and Streets, D. G.: Sources of black carbon aerosols in South Asia and surrounding
446 regions during the Integrated Campaign for Aerosols, Gases and Radiation Budget (ICARB), *Atmos. Chem.*
447 *Phys.*, 15, 5415-5428, <https://doi.org/10.5194/acp-15-5415-2015>, 2015.

448 Kumar, R., Naja, M., Satheesh, S. K., Ojha, N., Joshi, H., Sarangi, T., Pant, P., Dumka, U. C., Hegde, P.,
449 and Venkataramani, S. (2011), Influences of the springtime northern Indian biomass burning over the central
450 Himalayas, *J. Geophys. Res.*, 116, D19302, doi:10.1029/2010JD015509.

451

452 Li, C., Bosch, C., Kang, S., Andersson, A., Chen, P., Zhang, Q., Cong, Z., Chen, B., Qin, D., and Gustafsson, Ö.:
453 Source of blackcarbon to the Himalayan-Tibetan Plateau glaciers, *Nat. Com-mun.*, 7, 12574,

454 <https://doi.org/10.1038/ncomms12574>, 2016a.

455 Li, C., Yan, F., Kang, S., Yan, C., Hu, Z., Chen, P., ... & Stubbins, A. (2021). Carbonaceous matter in the atmosphere
456 and glaciers of the Himalayas and the Tibetan plateau: An investigative review. *Environment International*, 146,
457 106281

458 Li, X., Kang, S., He, X., Qu, B., Tripathee, L., Jing, Z., Paudyal, R., Li, Y., Zhang, Y., Yan, F., Li, G. and Li, C.:
459 Light-absorbing impurities accelerate glacier melt in the Central Tibetan Plateau, *Sci. Total Environ.*,
460 doi:10.1016/j.scitotenv.2017.02.169, 2017.

461 Li, Yang, S. Kang, Xuelei Zhang, Jizu Chen, Julia Schmale, Xiaofei Li, Yulan Zhang, Hewen Niu, Zhongqin Li,
462 Xiang Qin, Xiaobo He, Wei Yang, Guoshuai Zhang, Shijin Wang, Lili Shao, Lide Tian. 2021. Black carbon and
463 dust in the Third Pole glaciers: Revaluated concentrations, mass absorption cross-sections and contributions to
464 glacier ablation. *Science of the Total Environment*, 789: 147746. <https://doi.org/10.1016/j.scitotenv.2021.147746>.

465 Marcovecchio, A., Behrangi, A., Dong, X., Xi, B., Huang, Y. Precipitation Influence on and Response to Early and
466 Late Arctic Sea Ice Melt Onset During Melt Season. *International Journal of Climatology*

467 Mayer C, Lambrecht A, Belo` M, Smiraglia C and Diolaiuti G.: Glaciological characteristics of the ablation zone of
468 Baltoro glacier, Karakoram, Pakistan. *Ann. Glaciol.*, 43, 123–131, doi: 10.3189/172756406781812087, 2006

469 Niu, H., Kang, S., Wang, H., Du, J., Pu, T., Zhang, G., Lu, X., Yan, X., Wang, S., Shi, X., 2020. Light-absorbing
470 impurities accelerating glacial melting in southeastern Tibetan Plateau. *Environ. Poll.* 257, 113541.
471 <https://doi.org/10.1016/j.envpol.2019.113541>.

472 Rai M., Mahapatra P.S., Gul C. et al., Aerosol Radiative Forcing Estimation over a Remote High-altitude Location
473 (~4900 masl) near Yala Glacier, Nepal, *journal of Aerosol and Air Quality Research*, 19: 1872–1891, doi:
474 10.4209/aaqr.2018.09.0342, 2019

475 Pepin N C and Lundquist J D 2008 Temperature trends at high elevations: patterns across the globe *Geophys. Res.*
476 *Lett.* 35 L14701

477 Qian, Y., Flanner, M. G., Leung, L. R. and Wang, W. 2011. Sensitivity studies on the impacts of Tibetan Plateau
478 snowpack pollution on the Asian hydrological cycle and monsoon climate. *Atmos. Chem. Phys.* 11, 1929-1948.

479 Qian, Y., Wang, H., Zhang, R., Flanner, M. G., & Rasch, P. J. (2014). A sensitivity study on modeling black carbon
480 in snow and its radiative forcing over the Arctic and Northern China. *Environmental Research Letters*, 9(6),
481 064001.

482 Qu, B., Ming, J., Kang, S. C., Zhang, G. S., Li, Y. W., Li, C. D., Zhao, S. Y., Ji, Z. M. and Cao, J. J.: The decreasing
483 albedo of the Zhadang glacier on western Nyainqentanglha and the role of light-absorbing impurities, *Atmos.*
484 *Chem. Phys.*, 14(20), 11117–11128, doi:10.5194/acp-14-11117-2014, 2014.

485 Quinn, P. K., Bates, T. S., Baum, E., Doubleday, N., Fiore, A. M., Flanner, M., Fridlind, A., Garrett, T. J., Koch, D.,
486 Menon, S., Shindell, D., Stohl, A., and Warren, S. G.: Short-lived pollutants in the Arctic: their climate impact
487 and possible mitigation strategies, *Atmos. Chem. Phys.*, 8, 1723–1735, doi:10.5194/acp-8-1723-2008, 2008.

488 Ramanathan, V., and Carmichael, G.: Global and regional cli- mate changes due to black carbon, *Nat. Geosci.*, 1,
489 221–227, doi:10.1038/Ngeo156, 2008.

490 Ricchiazzi, P., Yang, S. R., Gautier, C., and Sowle, D.: SBDART: A research and teaching software tool for plane-

491 parallel radiative transfer in the Earth's atmosphere, *B. Am. Meteorol. Soc.*, 79, 2101–2114, 1998.

492 Schmale, J., Flanner, M., Kang, S., Sprenger, M., Zhang, Q., Guo, J., Li, Y., Schwikowski, M., Farinotti, D., 2017.

493 Modulation of snow reflectance and snowmelt from Central Asian glaciers by anthropogenic black carbon. *Sci.*

494 *Rep.* 7, 40501. <https://doi.org/10.1038/srep40501>.

495 Vaux, H. J., Jr., Balk, D., Cook, E. R., Gleick, P., Lau, W. K.-M. et al.: *Himalayan Glaciers: Climate Change, Water*

496 *Resources, and Water Security*. National Academies Press, Washington, DC, 2012.

497 Wang, X., Pu, W., Ren, Y., Zhang, X., Zhang, X., Shi, J., Jin, H., Dai, M. and Chen, Q.: Snow albedo reduction in

498 seasonal snow due to anthropogenic dust and carbonaceous aerosols across northern China, *Atmos. Chem. Phys.*

499 *Discuss.*, (September), 1–52, doi:10.5194/acp-2016-667, 2016.

500 Wang, Y., Ma, P.L., Peng, J., Zhang, R., Jiang, J.H., Easter, R.C., Yung, Y.L., 2018. Constraining aging processes of

501 black carbon in the community atmosphere model using environmental chamber measurements. *J. Adv. Model.*

502 *Earth Syst.* 10 (10), 2514e2526. <https://doi.org/10.1029/2018MS001387>.

503 Warren, S. G., and R. E. Brandt.: Optical constants of ice from the ultraviolet to the microwave: A revised

504 compilation, *J. Geophys. Res.*, 113, D14220, doi:10.1029/2007JD009744, 2008.

505 Xu, B., Cao, J., Joswiak, D. R., Liu, X., Zhao, H. and He, J.: Post-depositional enrichment of black soot in snow-

506 pack and accelerated melting of Tibetan glaciers, *Environ. Res. Lett.*, 7(1), 14022, doi:10.1088/1748-

507 9326/7/1/014022, 2012.

508 Yang, S., Xu, B., Cao, J., Zender, C. S. and Wang, M.: Climate effect of black carbon aerosol in a Tibetan Plateau

509 glacier, *Atmos. Environ.*, 111, 71–78, doi:10.1016/j.atmosenv.2015.03.016, 2015.

510 Yasunari, T. J., Koster, R. D., Lau, W. K. M., and Kim, K.: Impact of snow darkening via dust, black carbon, and

511 organic carbon on boreal spring climate in the Earth system, *J. Geophys. Res.-Atmos.*, 120, 5485–5503,

512 <https://doi.org/10.1002/2014JD022977>, 2015.

513 Yasunari, T. J., Bonasoni, P., Laj, P., Fujita, K., Vuillermoz, E., Marinoni, A., Cristofanelli, P., Duchi, R., Tartari, G.

514 and Lau, K. M.: Estimated impact of black carbon deposition during pre-monsoon season from Nepal Climate

515 Observatory - Pyramid data and snow albedo changes over Himalayan glaciers, *Atmos. Chem. Phys.*, 10(14),

516 6603–6615, doi:10.5194/acp-10-6603-2010, 2010.

517 Yao, T., Xue, Y., Chen, D., Chen, F., Thompson, L., Cui, P., Koike, T., Lau, W. K., Lettenmaier, D., Mosbrugger, V.,

518 Zhang, R., Xu, B., Dozier, J., Gillespie, T., Gu, Y., Kang, S., Piao, S., Sugimoto, S., Ueno, K., Wang, L., Wang,

519 W., Zhang, F., Sheng, Y., Guo, W., , Yang, X., Ma, Y., Shen, S. S. P., Su, Z., Chen, F., Liang, S., Liu, Y., Singh, V.

520 P., Yang, K., Yang, D., Zhao, X., Qian, Y., Zhang, Y., & Li, Q. (2019). Recent Third Pole's Rapid Warming

521 Accompanies Cryospheric Melt and Water Cycle Intensification and Interactions between Monsoon and

522 Environment: Multidisciplinary Approach with Observations, Modeling, and Analysis, *Bulletin of the American*

523 *Meteorological Society*, 100(3), 423-444. Retrieved Nov 1, 2021,

524 from <https://journals.ametsoc.org/view/journals/bams/100/3/bams-d-17-0057.1.xml>

525 You Q., Z. Cai, Nick Pepin, Deliang Chen, Bodo Ahrens, Zhihong Jiang, Fangying Wu, Shichang Kang, Ruonan

526 Zhang, Tonghua Wu, Pengling Wang, Mingcai Li, Zhiyan Zuo, Yanhong Gao, Panmao Zhai, Yuqing Zhang.

527 Warming amplification over the Arctic Pole and Third Pole: Trends, mechanisms and consequences. *Earth-*

528 Science Reviews, 217: 103625. <https://doi.org/10.1016/j.earscirev.2021.103625>.

529 Zaveri, R., Easter, R., Fast, J., and Peters, L.: Model for simulating aerosol interactions and chemistry (MOSAIC), J.

530 Geophys. Res., 113, D13204, doi:10.1029/2007JD008782, 2008.

531 Zhang, Q., Kang, S., Kaspari, S., Li, C., Qin, D., Mayewski, P. A., and Hou, S.: Rare earth elements in an ice core

532 from Mt. Everest: Seasonal variations and potential sources, Atmos. Res., 94, 300– 312, 2009.

533 Zhang, X. L., Wu, G. J., Kokhanovsky, A., Yao, T. D., and Tong D.: Spectral albedo parameterization for dirty snow

534 with considering mirco-physicochemical properties of impurities - Part I: Theory and preliminary evaluation,

535 2016

536 Zhang, Y., Kang, S., Xu, M., Sprenger, M., Gao, T., Cong, Z., Li, C., Guo, J., Xu, Z., Li, Y., Li, G., Li, X., Liu, Y.

537 and Han, H.: Light-absorbing impurities on Keqikaer Glacier in western Tien Shan : concentrations and potential

538 impact on albedo reduction, Sciences in Cold and Arid Regions, 9(2), doi:10.3724/SP.J.1226.2017.00097. 2017.

539 Zhang Y. L., S. Kang, M. Sprenger, Z. Cong, T. Gao, C. Li, S. Tao, X. Li, X. Zhong, M. Xu, W. Meng, B.

540 Neupane, X. Qin, M. Sillanpää. 2018. Black carbon and mineral dust in snow cover on the Tibetan Plateau. The

541 Cryosphere, 12: 413-431. <https://doi.org/10.5194/tc-12-413-2018>.

542

543 Zhao, C., Hu, Z., Qian, Y., Ruby Leung, L., Huang, J., Huang, M., Jin, J., Flanner, M. G., Zhang, R., Wang, H., Yan,

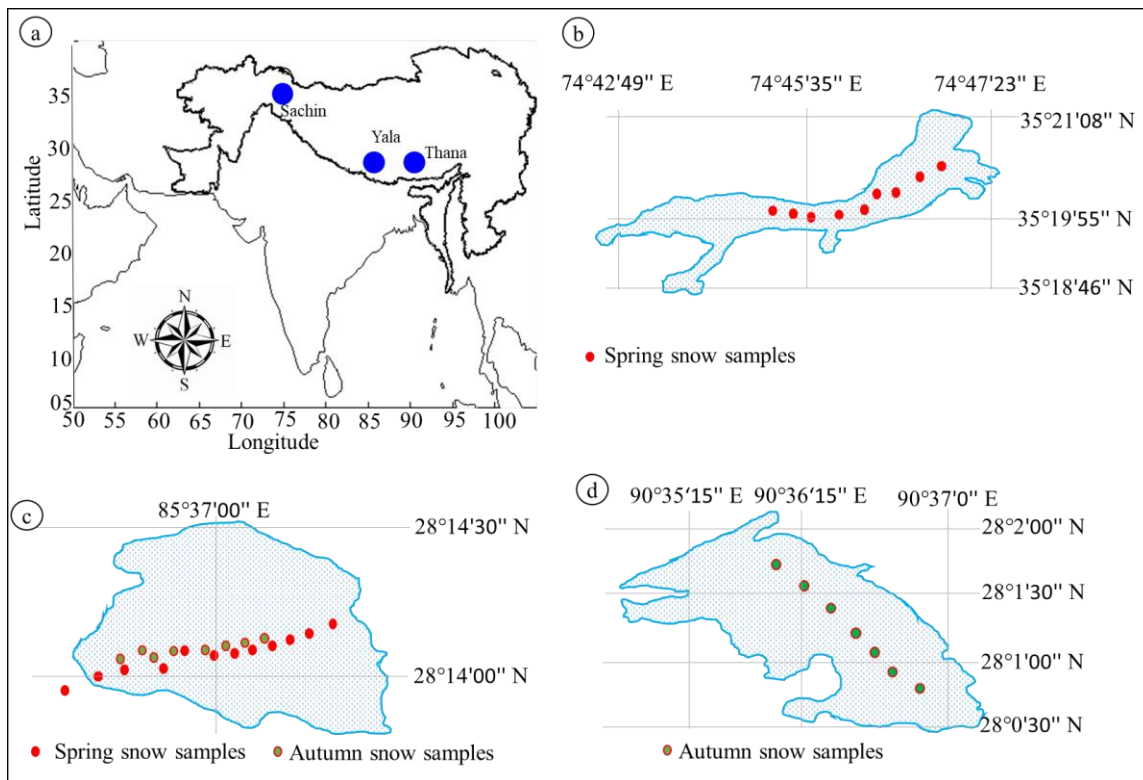
544 H., Lu, Z., and Streets, D. G.: Simulating black carbon and dust and their radia- tive forcing in seasonal snow: a

545 case study over North China with field campaign measurements, Atmos. Chem. Phys., 14, 11475– 11491,

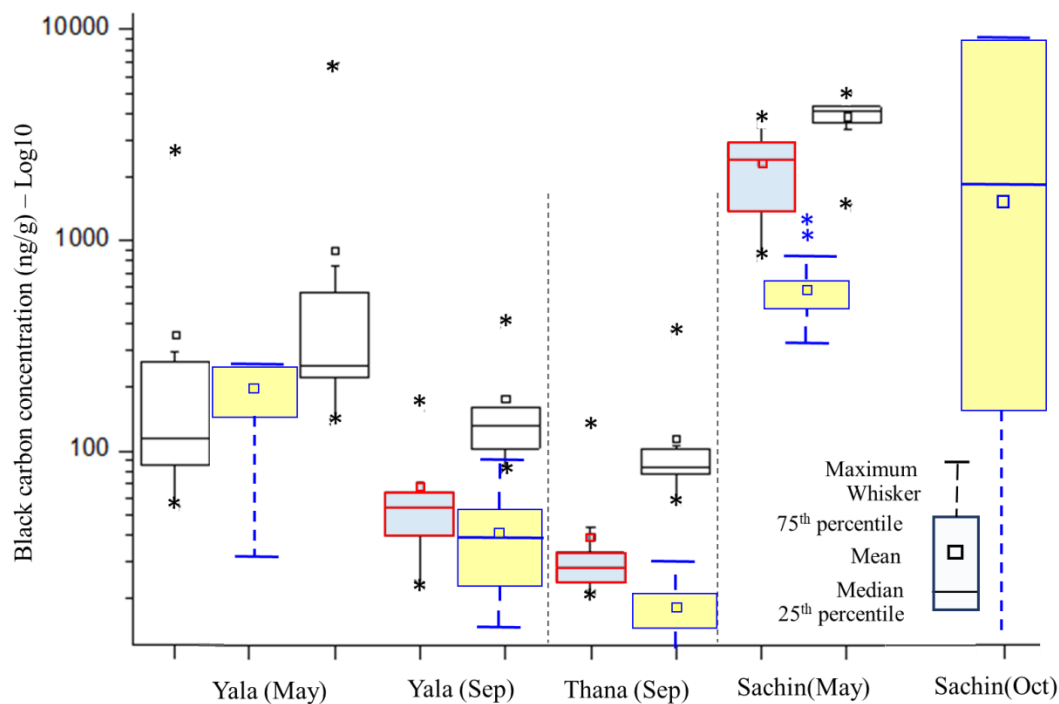
546 <https://doi.org/10.5194/acp-14-11475-2014>, 2014.

547

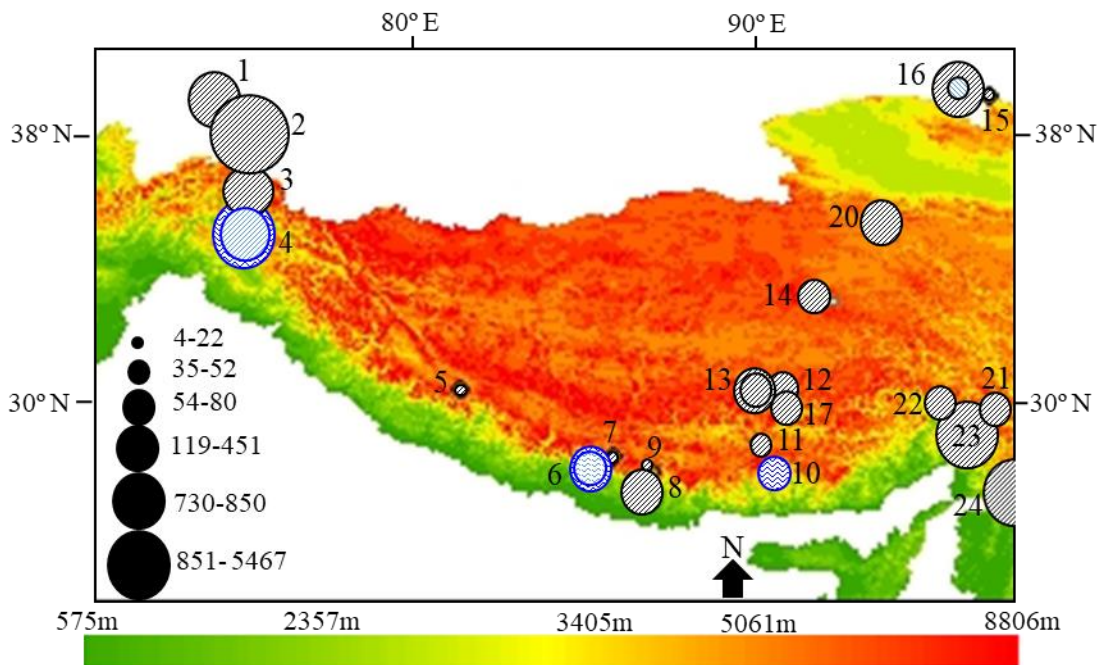
548



549
 550 **Fig. 1. Study area map (a) locations of selected glaciers in Himalaya Karakoram and Hindu Kush region (b) Sachin**
 551 **glacier in Pakistan (c) Yala glacier in Nepal (d) Thana glacier in Bhutan**
 552



553
 554 **Fig. 2. Whisker plots of black carbon (red box) and organic carbon (black box) concentrations (ngg^{-1}) in snow samples**
 555 **collected from three different glaciers in spring and autumn 2016. The yellow boxes are representing BC content in**
 556 **surface snow from WRF-Chem simulations. Stars (*) are representing outliers.**

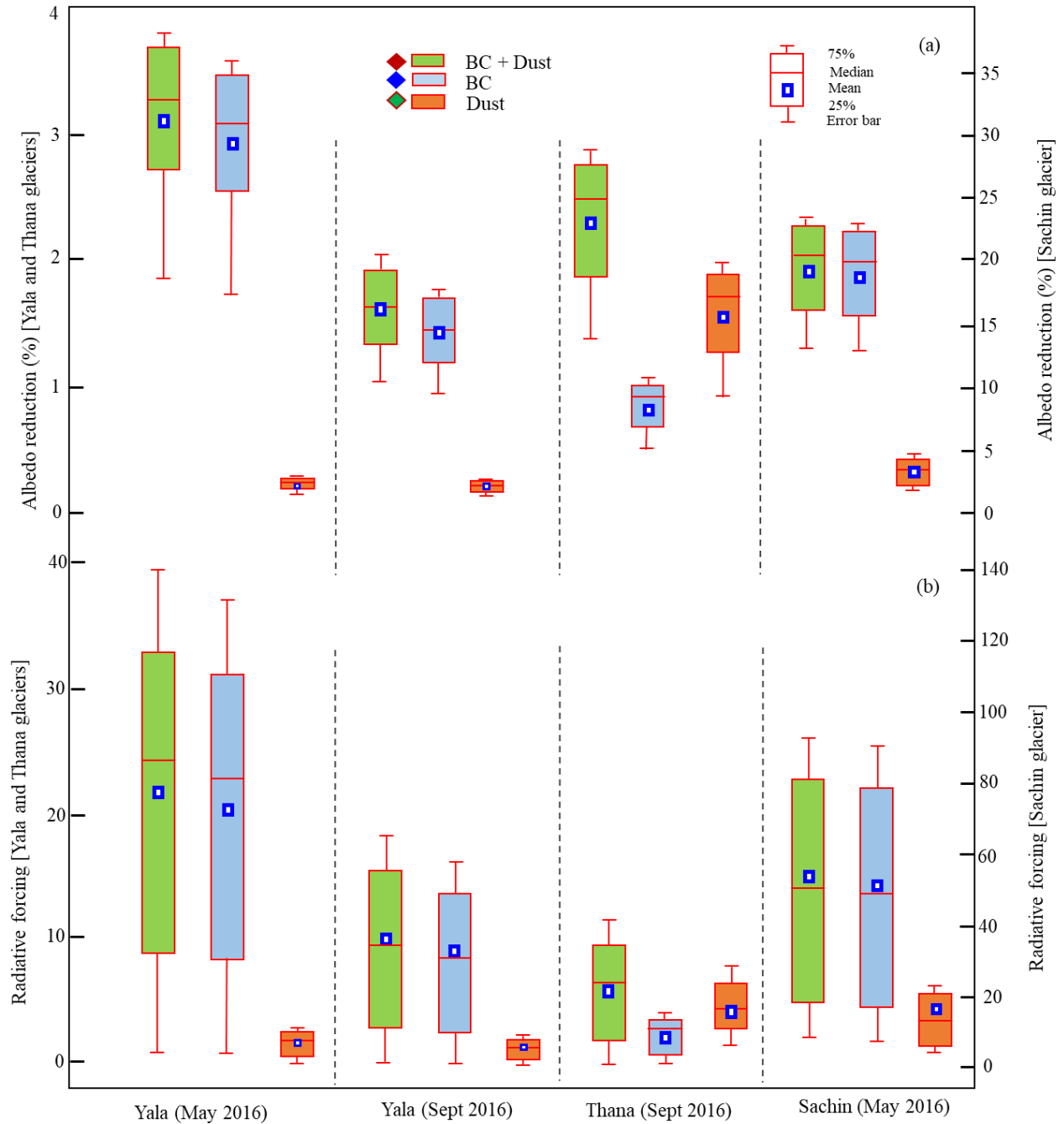


1. Muji (Yang 2015) 8. Mera (Kaspari 2014) 15. Qiyi (Xu 2006)
2. Muztagh Ata (Schmale 2017) 9. East Rongbuk (Ming 2009) 16. LHG (Li 2016, Ming 2009)
3. Gulkin (Gul 2018) 10. Thana (This study) 17. Lanong (Ming 2009)
4. Sachin (This study) 11. Qiangyong (Ming 2009) 20. Meikuang (Xu 2006)
5. Namunani (Xu 2006) 12. Xiaodongkemadi (Li 2017a) 21, 22, 23. Demula, Yarlong, Renlongba (Zhang 2017)
6. Yala (This study) 13. Zhadang (Ming 2009, Que 2014) 24. Mt. Yulong (Niu 2020)
7. Kangwure (Xu 2006) 14. DK (Xu 2006)

557

558 **Fig. 3. Black carbon concentrations (ng/g) in snow/ice samples in Himalayan, Karakoram and Tibetan Plateau in**
 559 **previous studies (black circles) and this study (blue circles).**

560

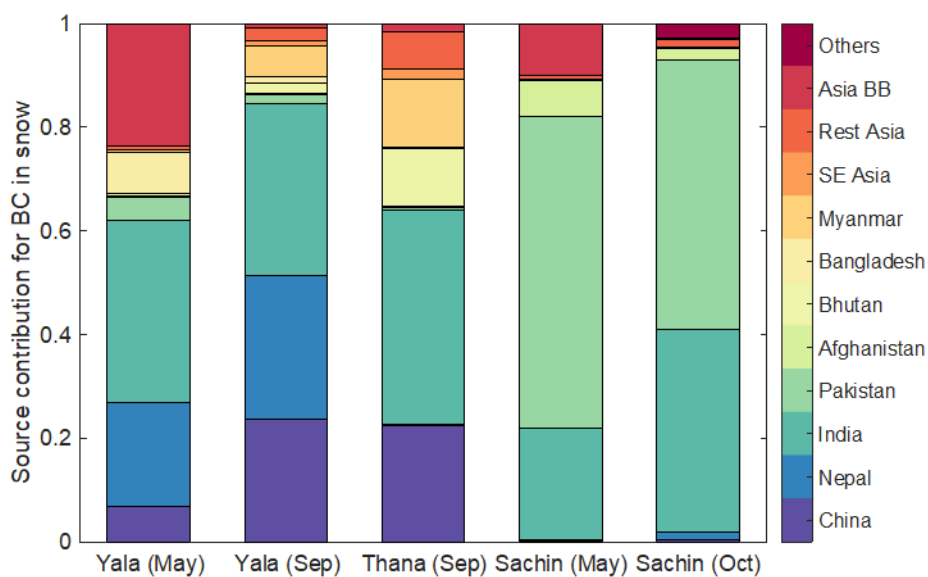


561

562 **Fig. 4. (a) Snow albedo reduction due to black carbon, dust and combined (black carbon and dust) during day time for a**
 563 **range of solar zenith angles. (b) Average instantaneous radiative forcing based on albedo reduction values during day**
 564 **time.**

565

566



567
 568 **Fig. 5. Source contributions to BC content in surface snow from WRF-Chem simulations at the three measurement**
 569 **glacier sites during the measurement periods. Source regions include anthropogenic emissions from China, India, Nepal,**
 570 **Pakistan, Afghanistan, Bhutan, Bangladesh, Myanmar, Southeast (SE) Asia, and the rest of Asia, as well as Asian biomass**
 571 **burning (BB) and BC transported from areas outside the study domain (Others).**

572

573

574

575 **Table 1. Snow sampling time and locations from selected glaciers**

Glacier	Lat/Long	Sampling date	Average elevation	Himalayas
Yala (Nepal)	28° 14' 12.25"N, 85° 37' 04.24"E	4 th - 7 th May 2016	4950 meters	Central
Yala (Nepal)	28° 14' 12.25"N, 85° 37' 04.24"E	29 th September 2016	4950 meters	Central
Thana (Bhutan)	28° 01' 22.23"N, 90° 36' 28.72"E	15 th September 2016	5400 meters	Central
Sachin (Pakistan)	35° 19' 55"N, 74° 45' 35"E	15 th May 2016	3230 meters	Western

576

577 **Table 2. Comparison of BC mass concentration, albedo reduction, radiative forcing and potential source regions of**
 578 **pollutants for central and western Himalayan glaciers during the study period**

	Central Himalaya min – max (average)	Western Himalaya min – max (average)	Time period
Monthly mean temperature (°C)	2.05-14.36(10.35) Yala -9.11- 5.68(0.23) Thana	-10.78 - 14.63 (3.57) Sachin	Apr 2015- Oct 2017
Monthly mean precipitation (mm day ⁻¹)	0.04536 - 41.472 Yala 1.0195 - 50.112 Thana	0.1546 - 5.866 (Sachin)	Apr 2015- Oct 2017
Monthly mean precipitation (mm), during sampling months	(4) Yala + Thana (29) Yala + Thana	(4) Sachin (3) Sachin	Apr 2016 Sep 2016
Elevation of sampling location (meters)	4580-5675 (5127)	3134-3957(3545)	
Observed BC in surface snow (ng g ⁻¹)	21 – 2529 (~350)	835 – 3545 (~2300)	2016
Albedo reduction (%) due to	0.13-3.82	12.00-24.00	2016

BC particles in snow			
Instantaneous radiative forcing (W m ⁻²) due to BC particles	0.0-39.65	0.03 to 96.48	2016
Potential source regions of pollutants			
3. WRF-Chem simulations	For the Yala site, it is dominated (>50%) by anthropogenic emissions from India and Nepal for both May and October, while the biomass burning contribution (>20%) increases largely in May. For the Thana site, it is dominated (>60%) by anthropogenic emissions from China and India in September, while anthropogenic emissions from Bhutan and Myanmar also contribute about 10%, respectively.	For the Sachin site, it is predominantly affected by anthropogenic emissions from India and Pakistan (total contribution >80%), while the spring biomass burning only contributes to ~10% in May.	

579
580